Supplementary Information

High efficiency two-photon uncaging by correction of spontaneous hydrolysis

Dénes Pálfi,[‡a,b] Balázs Chiovini,[‡a,b] Gergely Szalay,[b] Attila Kaszás,[b,c] Gergely F. Turi,[b,d] Gergely Katona,[a,b] Péter Ábrányi-Balogh,[e] Milán Szőri,[f] Attila Potor,[g] Orsolya Frigyesi,[a,g] Csilla Lukácsné Haveland,[a,g] Zoltán Szadai,[b,i] Miklós Madarász,[b,i] Anikó Vasanits-Zsigrai,[i] Ibolya Molnár-Perl,[i] Béla Viskolcz,[f] Imre G. Csizmadia,[j] Zoltán Mucsi*[b,j] and Balázs Rózsa[a,b]

[a] *Two-Photon Measurement Technology Research Group, The Faculty of Information Technology, Pázmány Péter Catholic University, Práter str 50, H-1083 Budapest, Hungary*
[b] *3D functional network and dendritic imaging, Institute of Experimental Medicine, Hungarian Academy of Sciences, Szigony str. 43, H-1083 Budapest, Hungary*
[c] *Institut de Neurosciences de la Timone Faculté de Médecine 27, boulevard Jean Moulin 13005 Marseille - France*
[d] *Department of Psychiatry, Columbia University, New York, NY 10032, USA*
[e] *Research Centre for Natural Sciences, Hungarian Academy of Sciences, Magyar tudósok krt. 2, H-1117 Budapest, Hungary*
[f] *Institute of Chemistry, Faculty of Materials Science and Engineering, University of Miskolc, H-3515 Miskolc, Hungary*
[g] *Femtonics LTD, Tuzolto utca 59, H-1094 Budapest, Hungary*
[h] *Department of Analytical Chemistry, Institute of Chemistry, Eötvös University, Pázmány Péter Sétány 1/A, 1117, Budapest, Hungary*
[I] *János Szentágothai PhD Program of Semmelweis University, H-1085 Budapest, Hungary*
[j] *Department of Chemistry, University of Toronto, Toronto, ON, Canada, M5S 3H6.*
‡ These co-first authors contributed equally to this work.

Correspondence should be addressed to Zoltán Mucsi: zoltanmucsi@gmail.com,
Institute of Experimental Medicine, Hungarian Academy of Sciences
Szigony u. 43., H-1083 Budapest, Hungary
Tel: (36)-30-3257771 Fax: (36)-1-2109423

***Keywords**: two-photon, uncaging, caged neurotransmitters, glutamate dehydrogenase, enzymatic elimination, reaction mechanism*

SUPPLEMENTARY METHODS

Materials and methods:

Amino acid derivatives were obtained from Bachem. All other chemicals were purchased from Sigma-Aldrich. Reagents were of the highest purity available. ^{1}H and ^{13}C-NMR spectra were recorded in DMSO-d_6 using TMS as an internal reference with a Bruker Avance III spectrometer operating at 400 MHz and 125 MHz. High-resolution MS spectra were measured using an Shimadzu MS spectrometer. In some cases, preparative HPLC was applied on an Armen type instruments, on a Gemini 250×50.00 mm; 10 μm, C18, 110A column in 0.2% TFA in water (eluent A) and acetonitrile (eluent B) liquid phase, using the gradient method.

Slice preparation and electrophysiology

Experiments were performed in accordance with the Hungarian Act of Animal Care and Experimentation (1998; XXVIII, section 243/1998.). The Animal Care and Experimentation Committee of the Institute of Experimental Medicine of the Hungarian Academy of Sciences, and the Animal Health and Food Control Station approved the experimental design. Acute hippocampal slices were prepared from 15-20-day-old rats and mice using isoflurane anesthesia followed by swift decapitation. Horizontal (300 μm) brain slices were cut with a vibratome and stored at room temperature in artificial cerebrospinal fluid (ACSF) (in mM: 126 NaCl, 2.5 KCl, 2 $CaCl_2$, 2 $MgCl_2$, 1.25 NaH_2PO_4, 26 $NaHCO_3$ and 10 glucose) as previously described.

Hippocampal neurons in CA1 stratum radiatum near the border of the stratum lacunosum-moleculare were visualized using 900 nm infrared oblique illumination. Whole-cell recordings were made at 32°C (MultiClamp 700B, Digidata 1440; Molecular Devices, Sunnyvale, CA, USA) with glass electrodes (current-clamp: 6–9 MΩ; voltage clamp: 3-5 MΩ) filled with (in mM): 125 K-gluconate, 20 KCl, 10 HEPES, 10 di-tris-salt phosphocreatine, 0.3 Na-GTP, 4 Mg-ATP, 10 NaCl, 0.1 Fluo-4, 0.1 ALEXA 594, and 0.008 biocytin. Cells with a resting membrane potential more negative than –50 mV were accepted. The recorded cells were classified as hippocampal interneurons and pyramidal cells according to their electrophysiological properties.

GABA IPSCs were induced by focal synaptic stimulation in the presence of AP5 (60 μM) and CNQX (10 μM). Glass electrodes (6-9 MΩ) filled with ACSF were placed at a distance of 10-15 μm from the soma (stimulation: 0.1 ms, 10-50 V, 10 ms pulse interval, 1 stimulus; BioStim, Supertech). All evoked IPSCs were verified for synaptic delay.

Data acquisition was performed using either pClamp8 or pClamp10 (Molecular Devices) and MES (Femtonics Ltd.) software.

Measurement of free glutamate concentration

Spontaneous hydrolysis of DNI-Glu•TFA was detected by direct measurement of glutamate concentration. Standard solutions of the glutamic acid were prepared with distilled water at concentrations of ~ 1.9–2.5·10^{-3} M (weighed with analytical precision) and further diluted before use. Stock solution of *o*-phthalaldehyde (OPA) contained 0.20 g (weighed with analytical precision) in 10 ml methanol (referred to as methanolic OPA solution). DNI-Glu•TFA (~0.01–0.014 g) was weighed with analytical precision and dissolved in 10 – 50 mL distilled water or in 12 mL ACSF (final concentration 2.5 mM for DNI-Glu•TFA). Borate buffer was mixed in 50/50 (v/v) ratios from 0.4 M boric acid (dissolved in 0.4 M potassium chloride) – 0.4 M sodium hydroxide. OPA/MPA reagents were obtained by mixing, in the order of listing, 500 μL methanolic OPA with 4 mL buffer solution and 20 μL MPA. 12 μL NADP solution (0.2 M) was added to the ACSF solution of DNI-Glu•TFA with or without the glutamate dehydrogenase enzyme. Different amounts of enzyme were added (200, 520, 1040, 2000 and 5200 units/L) to the 12 mL ACSF solution saturated with 95 % O_2 and 5 % CO_2 gas. Derivatizations of blank, standard, and sample solutions were performed with reagent solutions stored in the refrigerator no longer than < 9 days, at ~4 C°. 400 μL reagent solutions were mixed with 60 μL glutamic acid or DNI-Glu•TFA solutions and let react for 5 min before injection. The analytical setup consisted of a Waters HPLC instrument (Waters, Milford, MA, USA), made of a Waters 996 PDA Detector and a Waters 474 Detector, a Waters 616 Controller quaternary pump with a thermostattable column area, and a Waters 717 Autosampler, operating with the Millennium Software (version 2010, 1992–95, validated by ISO 9002). The analytical columns were a BST Hypersil ODS, 15 cm × 4.0 mm, 5 μm; a Thermo Hypersil ODS 15 cm × 4.6 mm, 5 μm; and a Thermo Hypersil Gold 20 cm × 4.6 mm, 5 μm, all three used with guard columns (BST Hypersil ODS 20 mm × 4 mm, 5 μm or Thermo Hypersil ODS 10 mm × 4 mm, 5 μm).

Detections were performed simultaneously: PDA and Fl detectors were connected in the order of listing. PDA data were recorded between 190 and 400 nm (PDA) and evaluated at 285 nm for DNI and 337 nm for all the OPA–caged-glutamate derivatives. The fluorescence intensities of the OPA–glutamic acid derivative were evaluated at the optimum fluorescence wavelengths of isoindoles ($\lambda_{Ex}/\lambda_{Em}$=337/454 nm).

The eluent system consisted of two components: eluent A was: 0.05 M sodium acetate of pH 7.20 ± 0.05, while eluent B was prepared from 0.1 M sodium acetate–acetonitril–methanol (46/44/10), mixed in volume ratios and titrated with glacial acetic acid or 1.0 M sodium hydroxide to pH 7.20 ± 0.05. Elutions were performed in the gradient mode (40 ^{0}C): starting with 1% B for 1 min with 1.3 ml/min flow rate, reaching 100% B and 2.0 ml/min flow rate within 7 minutes, afterwards 3 minutes isocratic elution with 100% B, and, finally, returning to the initial concentration (1% B) in 1 minute and equilibrating for 4 minutes with this B content.

OPA, MPA, glutamic acid, and glutamate dehydrogenase were obtained from Sigma (St. Louis, MO, USA). NADP was produced by Calbiochem (Germany, Darmstadt). HPLC-grade methanol and acetonitrile were purchased from Sigma-Aldrich (Seelze, Germany). Reagents were of the highest purity available.

Two-photon imaging

Two-photon imaging started 15–20 min after attaining the whole-cell configuration, on a two-photon laser-scanning system (Femto2D, Femtonics Ltd.) using femtosecond lasers (830-850 nm), (Mai Tai HP, SpectraPhysics). The Multiple Line Scanning Method was used to image long dendritic segments. At the end of each experiment, a series of images were taken across the depth of the volume encompassing the imaged neuron. Measurement control, real-time data acquisition and analysis were performed with a MATLAB-based program (MES, Femtonics Ltd.) and using a custom-written software.

Two-photon uncaging

After achieving whole-cell mode and filling pyramidal cells or interneurons with 100 μM Fluo-4, the bath solution was changed to ACSF containing 2.5 mM MNI-Glu•TFA (**1**), DNI-Glu•TFA (**2**), MNI-Ulg•TFA (**3**), or DNI-Ulg•TFA (**4**). Photolysis of caged glutamate was performed with 690-830 nm ultrafast, pulsed laser light (Mai Tai HP Deep See, SpectraPhysics or Cameleon Ultra II, Coherent). The intensity of the uncaging laser beam was controlled with an electro-optical modulator (Model 350-80 LA, Conoptics). Dispersion compensation was set to have maximal response at the depth of uncaging (50-80 μm from surface). The uncaging laser beam was coupled to the imaging optical pathway with a dichroic mirror (custom laser combiner, z750bcm; Chroma Technology Corp). Chromatic aberration was compensated for at the focal plane. Radial and axial alignment errors between the imaging and uncaging point spread functions were held with two motorized mirrors below 100 nm and 300 nm, respectively. Imaging was interleaved with two-photon glutamate uncaging periods when galvanometers jumped to 15-25 selected locations (within <60 μs jump time) and returned back to the imaging trajectory thereafter. Positions of uncaging sites were finely adjusted according to background images taken. Line scan data were also used to avoid overlapping between uncaging locations and the dendrite. Photolysis of caged glutamates was performed in “clustered” patterns (0.8±0.1 μm distance between inputs) along the dendrite. Small drifts of the sample (approximately 0.1-0.2 μm/min) were compensated manually according to regularly taken background images and fluorescent pixel intensities in uncaging

locations during photo-stimulation. The same uncaging pattern in the same dendritic location was used during comparison of different uncaging materials. Perfusion rate was set to 6 ml/min in order to increase the exchange rate of ACSF containing different uncaging materials. L-glutamic dehydrogenase (Sigma-Aldrich) was applied to the bath. β-nicotinamide adenine dinucleotide phosphate hydrate (200 μM, Sigma-Aldrich) was also applied to the bath, or alternatively, was injected with 1 μM/min with an initial concentration of 50-100 μM in order to compensate for consumption during the enzymatic reaction. Unless otherwise indicated, data are presented as mean±s.e.m. Statistical comparisons were performed using the Student's paired *t*-test.

Statistics

We measured the overall photochemical yields of DNI-Glu•TFA (**2**), DNI-Ulg•TFA (**4**), and MNI-Ulg•TFA relative to the responses of MNI-Glu•TFA by calculating the relative change in the second order of laser intensity (2p irradiation), which is required to generate overlap in the responses. We used unconstrained non-linear optimization to minimize the distance between the two point sets, where the changed variable was the scale factor applied to the 2p irradiation bringing the two point sets into overlap. The distance between the point sets was defined by the sum:

$$r = \sum_{i,j} \left(x_i - x_j\right) e^{-\left(y_i - y_j\right)^2 / S^2}$$

Where x_i and x_j are the laser intensity data corresponding to the two datasets, while y_i and y_j are the corresponding EPSP or Ca^{2+} transient amplitudes. S was set to 2 mV for EPSP, and 2 % for Ca^{2+} transient measurements (**Figure 8a**).

Computational methods

All computations were carried out with the Gaussian09 program package (G09), using convergence criteria of 3.0×10^{-4}, 4.5×10^{-4}, 1.2×10^{-3} and 1.8×10^{-3}, for the gradients of the root mean square (RMS) force, maximum force, RMS displacement, and maximum displacement vectors, respectively. Computations were carried out at B3LYP/6-31G(d,p) level of theory. As shown earlier, CH_2Cl_2 does not require consideration of the solvent effect during the modeling process. The method and basis sets were chosen for their reliability in agreement with the studies established earlier. The vibrational frequencies were computed at the same levels of theory, as used for geometry optimization, in order to properly confirm that all structures reside at minima on their potential energy hypersurfaces (PESs). Thermodynamic functions U, H, G, and S were computed at 298.15 K.

Since trifluoroacetic acid (TFA) is mainly important for crystallizing the caged neurotransmitters under biologically relevant conditions (pH=7.4), the solvated caged neurotransmitters are mostly in their zwitterionic form. Therefore, geometric optimization of these ionic caged neurotransmitters was carried out in the absence of TFA in aqueous phase mimicked by the CPCM continuum model of implicit water as implemented in the Gaussian09 software package (Revision A.1, 2009). To obtain only the real local minima of the B3LYP/6-31G(d,p) potential energy surface, normal mode analysis was carried out at the same level of theory, then the B3LYP/6-31G(d,p) harmonic frequencies obtained were used to evaluate the thermochemical properties ($\Delta H°$, $\Delta S°$ and $\Delta G°$) of the species studied. The solvation Gibbs free energy of these species, $\Delta G_{solv}{}^0$, was also calculated.

Based on these B3LYP/6-31G(d,p) geometries, the degenerated two-photon absorption strength for an average molecular orientation was computed at the same B3LYP/6-31G(d,p) level of theory *via* quadratic response theory.

Geometric optimizations and frequency calculations were performed with the Gaussian09 software package, while the time-dependent calculations of static non-linear properties were obtained using the DALTON 2.0 quantum chemistry program.

Detailed description of quantum molecular computed results

Three branching points exist in the mechanistic scheme (**Figures 3 and 10**).

Point I. The ratio of the processes from the ground state A(S_0) to the excited state B(S_1) and the spontaneous hydrolyzed J(S_0) compounds depends significantly on the experimental conditions, such as light intensity, temperature, and retention time of the compound in the experiment. In a general experiment, the typical ratio of the spontaneous hydrolysis for MNI-Glu is about 0.1%. Under the same experimental conditions, due to the 29-fold faster hydrolysis rate, about 3% of DNI-Glu hydrolyses spontaneously, and 97% is excited to the B(S_1) state.

Point II. The ratio of de-excitation processes from E(T_1) to H(S_0), and the triplet-state reaction of E(T_1) to F(T_1) was estimated by the relationship between the activation enthalpy [H(TS2)] of the process of E(T_1)→F(T_1) and the intercrossing enthalpy change [H(IC)] of the process E(T_1)→H(S_0). In this speculation, it is generally accepted that there is a linear relationship between the energy difference of the triplet and singlet surfaces and the intensity of intersystem crossing (IC); the smaller the energy difference, the higher the transformation rate.

$$\Delta H(TS2) = H\left[TS2(T_1)\right] - H\left[E(T_1)\right], \quad \textbf{Eq. S2}$$

$$\Delta H(IC) = H\left[E(T_1)\right] - H\left[H(S_0)\right], \quad \textbf{Eq. S3}$$

The activation barrier of the straightforward triplet reaction for MNI-Glu is 8.3 kJ mol^{-1} higher than that of DNI-Glu, directing the transformation to the "unwanted" IC process, mainly deactivating MNI-Glu by de-excitation. In the absence of general mathematical equations, it is difficult to estimate the ratio of the two processes. However, in the case of MNI-Glu, one can estimate that the transformation toward de-excitation should be about 10-fold faster than the "useful" triplet state reaction. For DNI-Glu, the same speculation shows an opposite picture, where the triplet state reaction is roughly 28 times faster, due to the lower H(TS2) enthalpy barrier (**Eq. S4**) as well as 2-times faster IC. Overall, one can estimate, that the DNI-Glu transformation toward to the position F(T_1) on the triplet surface is ten times more effective than MNI-Glu transformation, resulting in a 10-fold more effective process. A very different conclusion can be drawn for MNI-Ulg and DNI-Ulg, because the significantly higher barriers inhibit the formation of the photocleavaged products: therefore, the IC process dominates the mechanism. According to the QM calculations, only a very poor quantum yield can be assigned to the Ulg products.

Point III. The ratio of the rate of back-isomerisation [$H(S_0) \rightarrow A(S_0)$] and the spontaneous hydrolysis process [$H(S_0) \rightarrow J(S_0)$] can be estimated by their activation enthalpy difference, described in **Eq. S4-S7**. All of these ratios were rounded to 0.1% toward the hydrolysis, therefore the overall main process is the back process to the initial state $A(S_0)$. The same conclusion can be draw for MNI-Ulg and DNI-Ulg (**Eq. S8-S11)**.

$$\Delta H_{TS}(MNI\text{-}Glu) = H[TS6](MNI\text{-}Glu) - H[TS3](MNI\text{-}Glu) = 142.8 - 161.1 = \text{-}18.3 \frac{kJ}{mol}, \quad \textbf{Eq. S4}$$

$$ratio(MNI\text{-}Glu) = e^{\frac{\Delta H_{TS}(MNI\text{-}Glu)}{RT}} = e^{\frac{-18.3\,{}^{kJ}/_{mol}}{306K \times 0.008314\,{}^{kJ}/_{K*mol}}} = 0.000654 \approx 0.1\%, \quad \textbf{Eq. S5}$$

$$\Delta H_{TS}(DNI\text{-}Glu) = H[TS6](DNI\text{-}Glu) - H[TS3](DNI\text{-}Glu) = 138.9 - 158.6 = \text{-}19.7 \frac{kJ}{mol}, \quad \textbf{Eq. S6}$$

$$ratio(DNI\text{-}Glu) = e^{\frac{\Delta H_{TS}(DNI\text{-}Glu)}{RT}} = e^{\frac{-19.7\,{}^{kJ}/_{mol}}{306K \times 0.008314\,{}^{kJ}/_{K*mol}}} = 0.000371 \approx 0.1\%, \quad \textbf{Eq. S7}$$

$$\Delta H_{TS}(MNI\text{-}Ulg) = H[TS6](MNI\text{-}Ulg) - H[TS3](MNI\text{-}Ulg) = 167.3 - 185.5 = \text{-}18.2 \frac{kJ}{mol}, \quad \textbf{Eq. S8}$$

$$ratio(MNI\text{-}Ulg) = e^{\frac{\Delta H_{TS}(MNI\text{-}Ulg)}{RT}} = e^{\frac{-18.2\,{}^{kJ}/_{mol}}{306K \times 0.008314\,{}^{kJ}/_{K*mol}}} = 0.000658 \approx 0.1\%, \quad \textbf{Eq. S9}$$

$$\Delta H_{TS}(DNI\text{-}Ulg) = H[TS6](DNI\text{-}Ulg) - H[TS3](DNI\text{-}Ulg) = 157.9 - 178.2 = \text{-}20.3 \frac{kJ}{mol}, \quad \textbf{Eq. S10}$$

$$ratio(DNI\text{-}Ulg) = e^{\frac{\Delta H_{TS}(DNI\text{-}Ulg)}{RT}} = e^{\frac{-20.3\,{}^{kJ}/_{mol}}{306K \times 0.008314\,{}^{kJ}/_{K*mol}}} = 0.000152 \approx 0.1\%, \quad \textbf{Eq. S11}$$

MNI-Glu TFA (1)

HPLC-MS chromatogram and MS spectra:

Analytical Sheet

α-Amino-2,3-dihydro-4-methoxy-7-nitro-δ-oxo-1*H*-indole-1-pentanoic acid trifluoroacetate

Molecular formula: $C_{16}H_{18}F_3N_3O_8$ **Mw:** 437.32

The HPLC purity is within specifications (>98%): **The Mass spectrum is consistent with the structure**

Theoretical: C: 43,94%; H: 4.15%; N: 9.61%; **Found:** C: 43.68%; H: 3,92%; N: 9.43%;

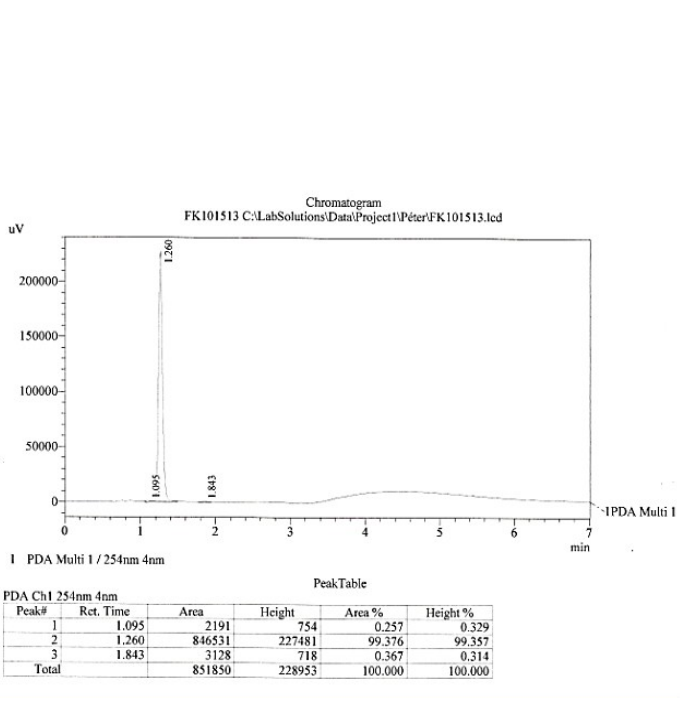

PeakTable

PDA Ch1 254nm 4nm

Peak#	Ret. Time	Area	Height	Area %	Height %
1	1.095	2191	754	0.257	0.329
2	1.260	846531	227481	99.376	99.357
3	1.843	3128	718	0.367	0.314
Total		851850	228953	100.000	100.000

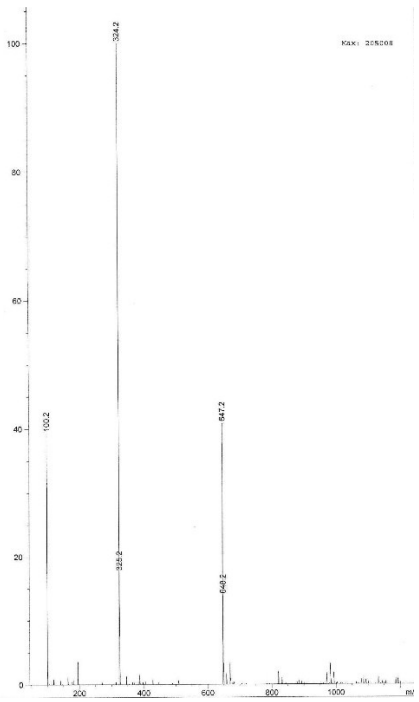

1H NMR spectra:

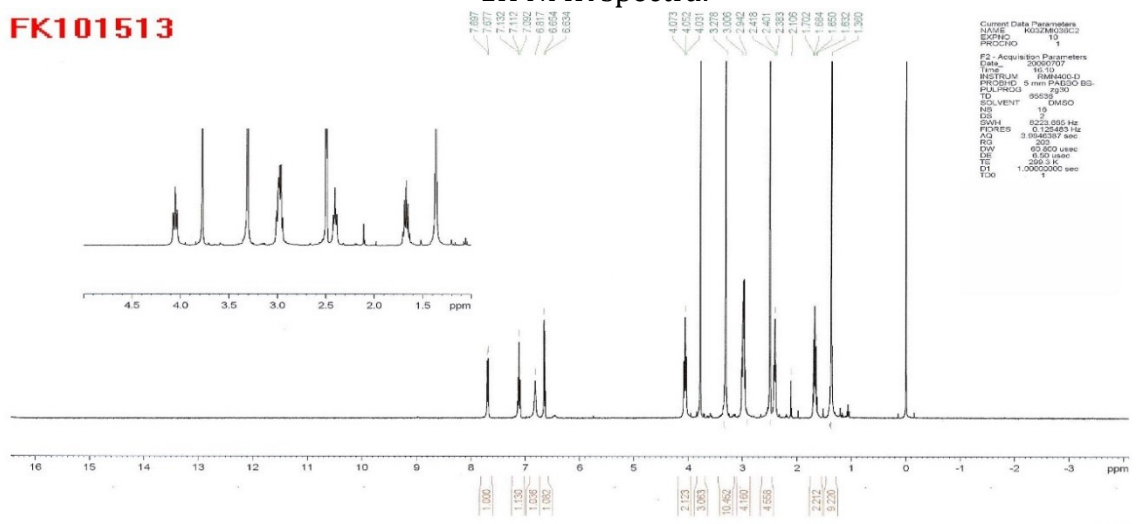

DNI-Glu TFA (2)

HPLC-MS chromatogram and MS spectra:

1H NMR spectra

Analytical Sheet

DNI-Glutamate Trifluoroacetate

α-Amino-2,3-dihydro-4-methoxy-5,7-dinitro-δ-oxo-1*H*-indole-1-pentanoic acid trifluoroacetate

Molecular formula: $C_{14}H_{17}N_4O_8 \times C_2F_3O_2$

MW: 482,32

Elem. Anal: **Theoretical:** C: 39,84%; H: 3,55%; N: 11,62%; **Found:** C: 39,63%; H: 3,47%; N: 11,59%;

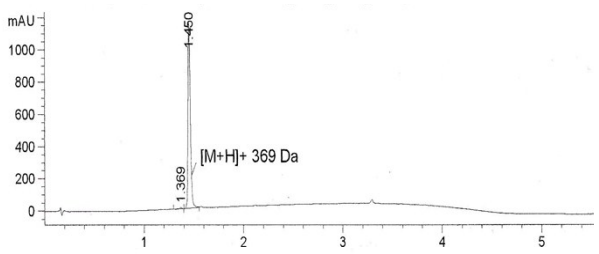

Signal 2: DAD1 B, Sig=280,16 Ref=off

Peak #	RetTime [min]	Type	Width [min]	Area [mAU*s]	Height [mAU]	Area %
1	1.450	BB	0.0264	919.11218	552.34845	100.0000

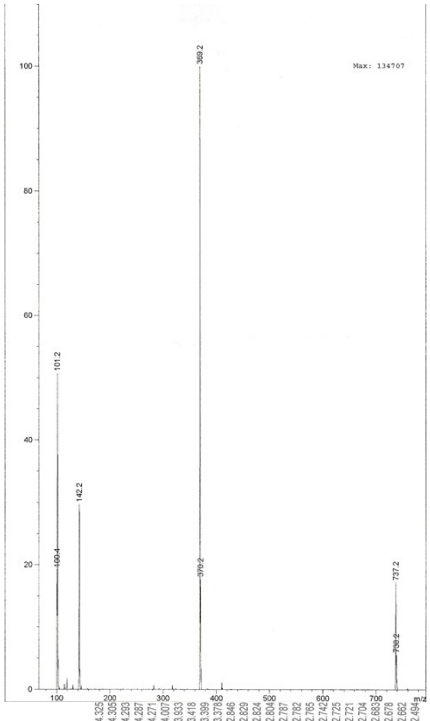

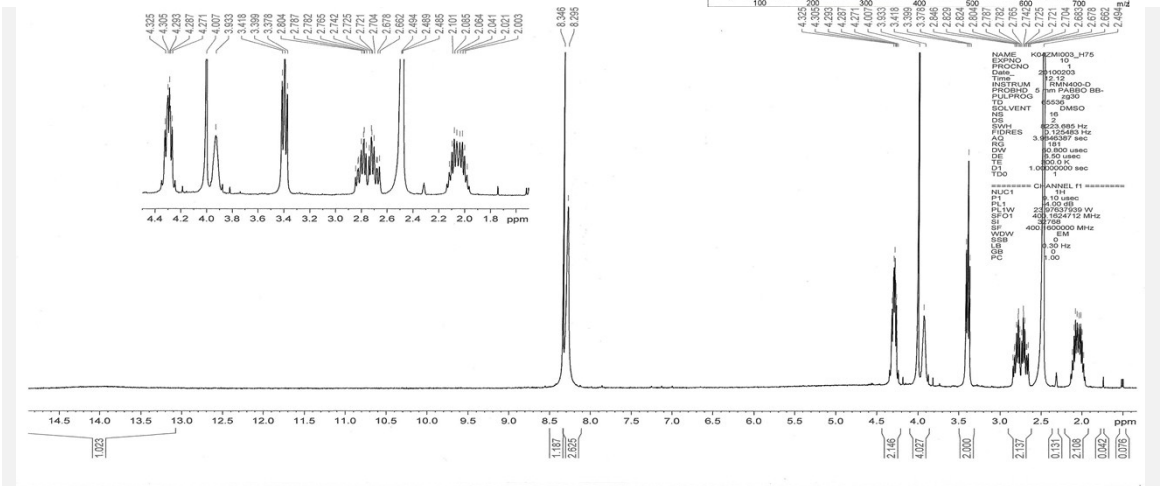

HPLC purity is within specifications (>98%): The mass spectrum is consistent with the structure^{1}H-NMR spectrum is consistent with the structure:

MNI-Ulg TFA (3)

HPLC-MS chromatogram and MS spectra:

Analytical Sheet

δ-Amino-2,3-dihydro-4-methoxy-7-nitro-α-oxo-1*H*-indole-1-pentanoic acid trifluoroacetate

Molecular formula: $C_{16}H_{18}F_3N_3O_8$ **Mw:** 437.32

The HPLC purity is within specifications (>98%): **The Mass spectrum is consistent with the structure**

Theoretical: C: 43,94%; H: 4.15%; N: 9.61%; **Found:** C: 43.42%; H: 3,89%; N: 9.36%;

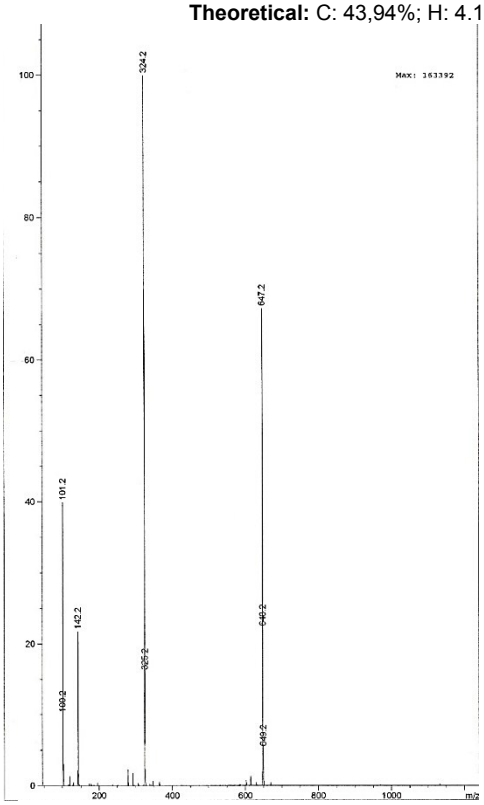

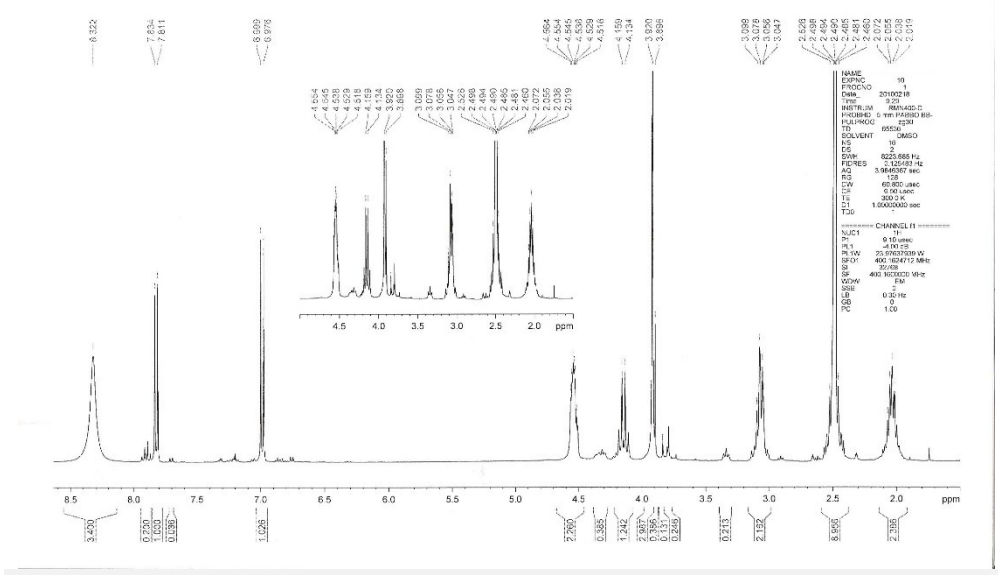

DNI-Ulg TFA (4)

HPLC-MS chromatogram and MS spectra:

1H NMR spectra

Analytical Sheet

DNI-Glutamate Trifluoroacetate

δ-Amino-2,3-dihydro-4-methoxy-5,7-dinitro-α-oxo-1*H*-indole-1-pentanoic acid trifluoroacetate

Molecular formula: $C_{14}H_{17}N_4O_8 \times C_2F_3O_2$

MW: 482,32

Elem. Anal: **Theoretical:** C: 39,84%; H: 3,55%; N: 11,62%; **Found:** C: 39,44%; H: 3,39%; N: 11,50%;

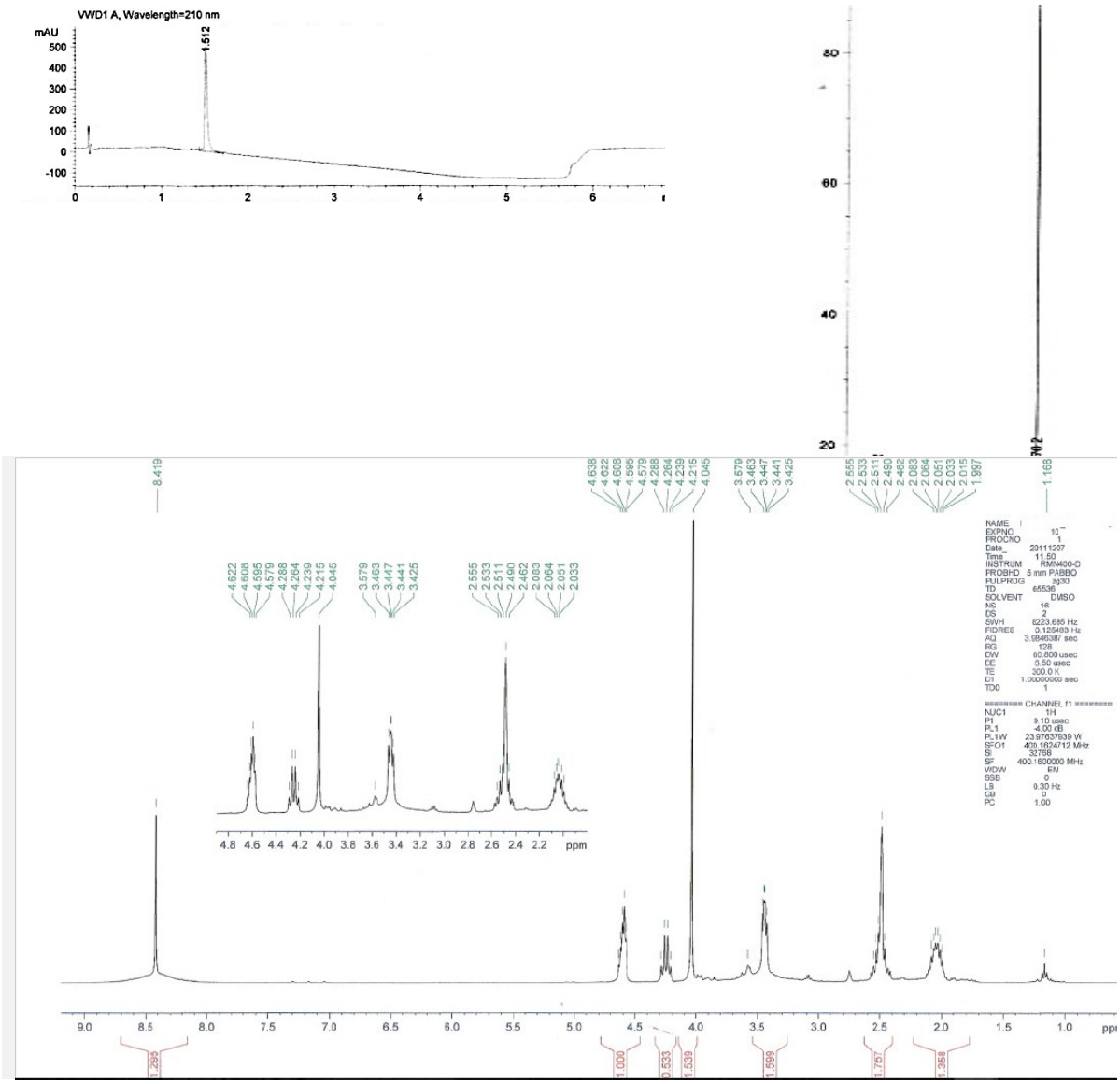

VI-Glu (10)
Tert-butyl 2-((tert-butoxycarbonyl)amino)-5-(4-methoxyindolin-1-yl)-5-oxopentanoate

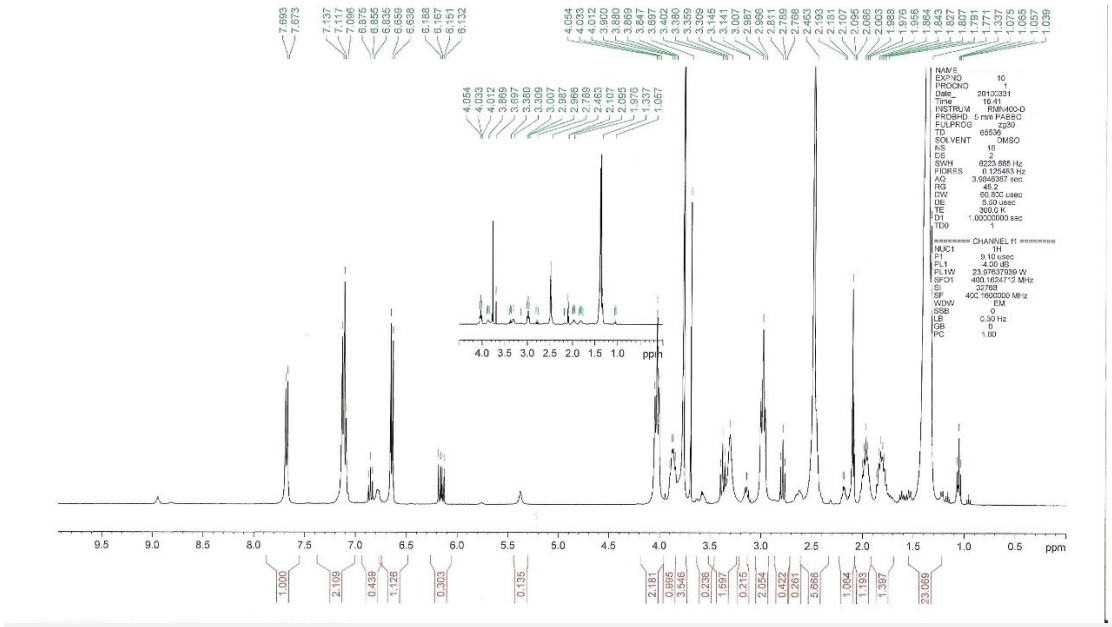

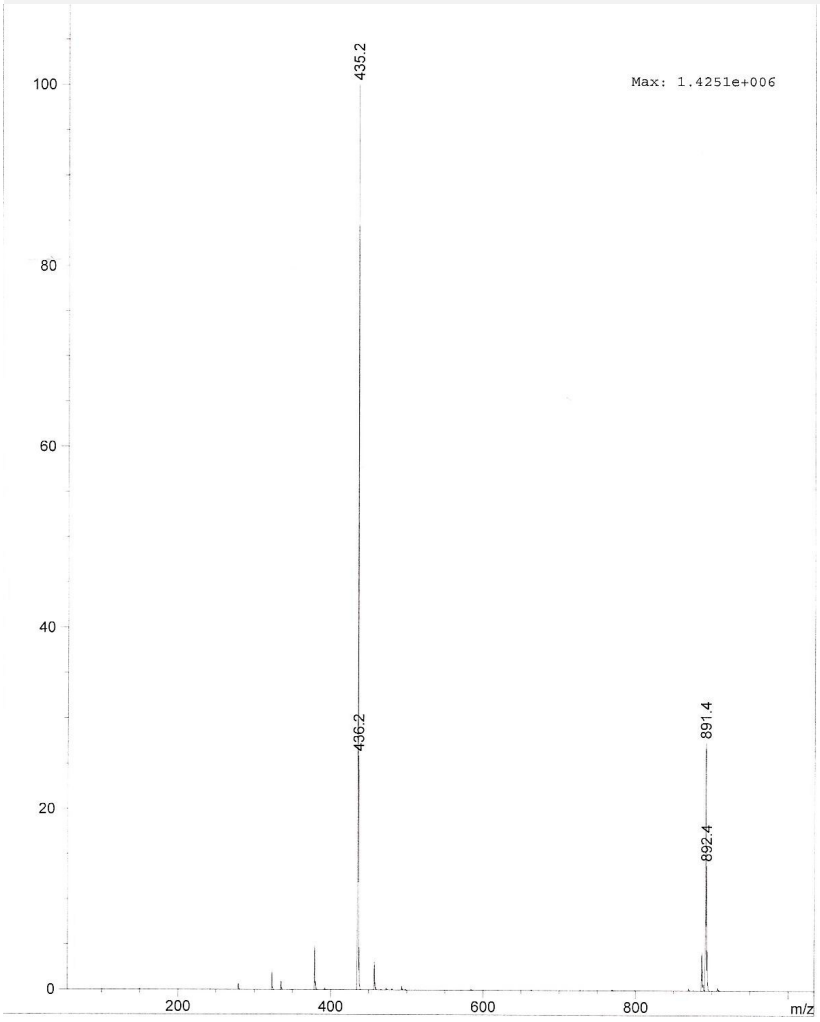

VI-Ulg (11)
Tert-butyl 4-((tert-butoxycarbonyl)amino)-5-(4-methoxyindolin-1-yl)-5-oxopentanoate

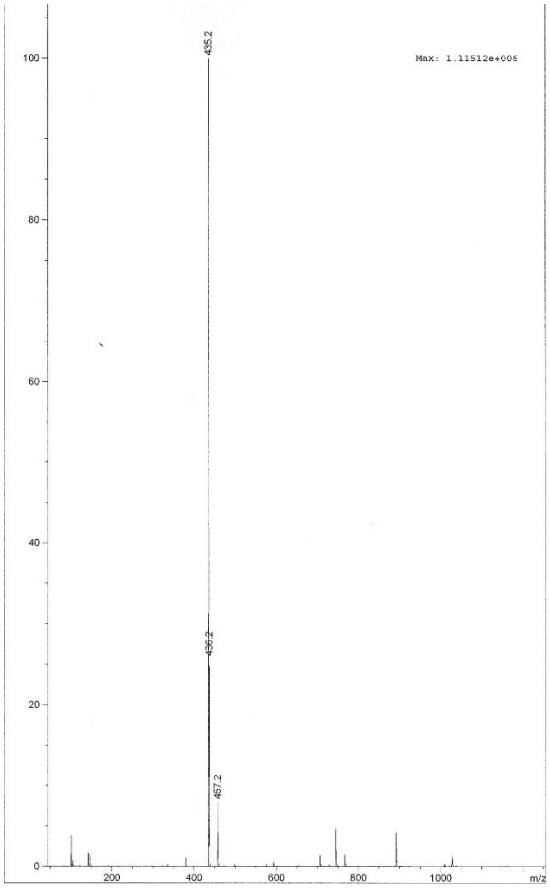

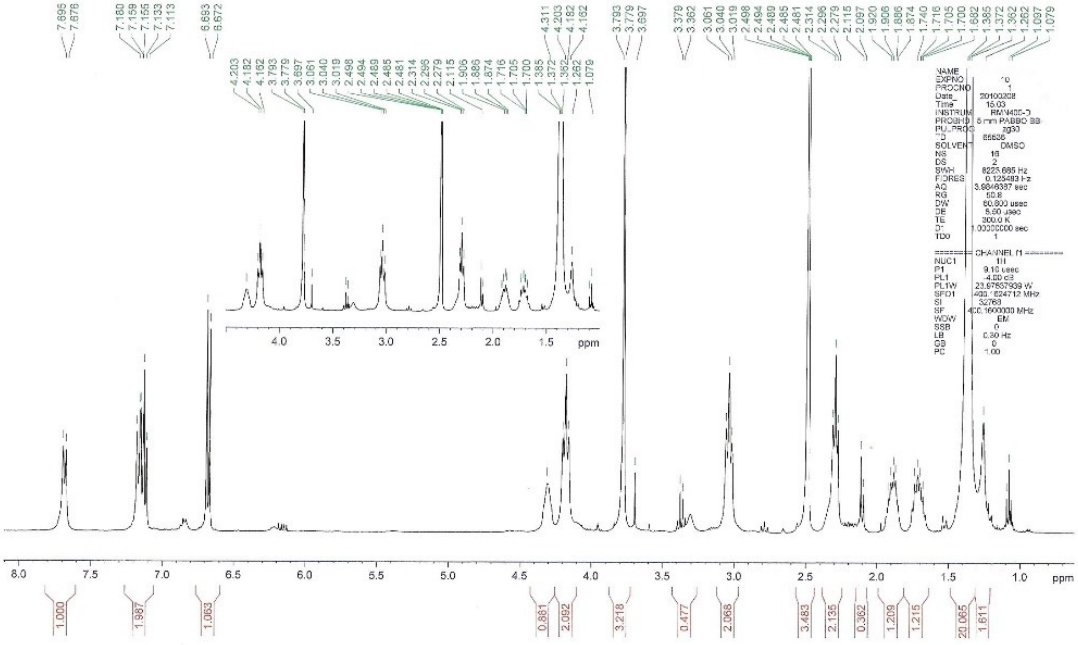

VMNI-Glu (12)
Tert-butyl 2-((tert-butoxycarbonyl)amino)-5-(4-methoxy-7-nitroindolin-1-yl)-5-oxopentanoate

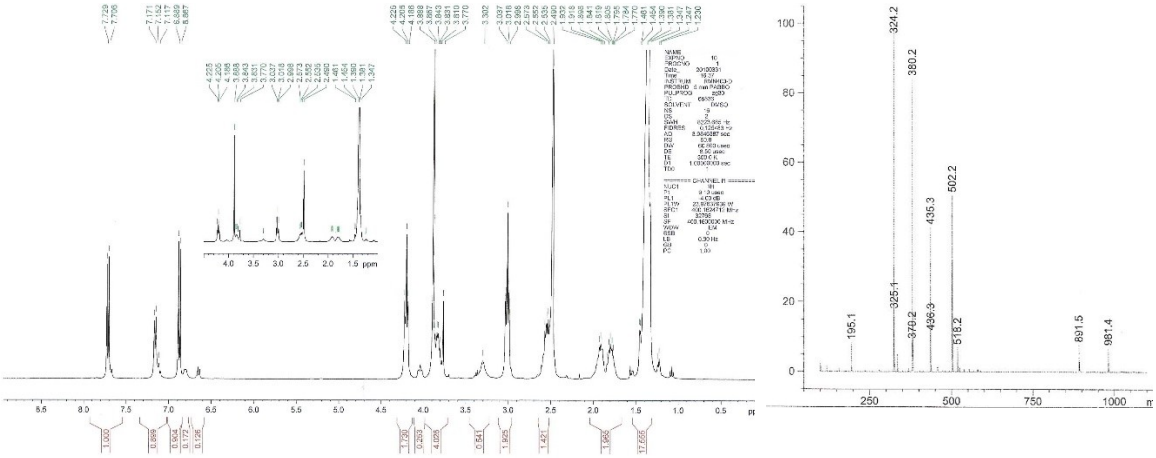

VMNI-Ulg (13)
Tert-butyl 4-((tert-butoxycarbonyl)amino)-5-(4-methoxy-7-nitroindolin-1-yl)-5-oxopentanoate